

2010-01-01

Visible Near-Infrared Hyperspectral Imaging for the Identification and Discrimination of Brown Blotch Disease on Mushroom (*Agaricus bisporus*) Caps

Edurne Gaston

Technological University Dublin, edurne.gaston@tudublin.ie

Jesus Maria Frias

Technological University Dublin, Jesus.Frias@tudublin.ie

Patrick Cullen

Technological University Dublin, pj.cullen@tudublin.ie

Follow this and additional works at: <https://arrow.tudublin.ie/schfsehart>

See next page for additional authors



Part of the [Agriculture Commons](#), and the [Food Processing Commons](#)

Recommended Citation

, Frias JM. et al. (2010) Visible-near infrared hyperspectral imaging for the identification and discrimination of brown blotch disease on mushroom (*Agaricus bisporus*) caps. *Journal of Near Infrared Spectroscopy* Volume 18 Issue 5, Pages 341–353. doi.org/10.1255/jnirs.894

This Article is brought to you for free and open access by the School of Food Science and Environmental Health at ARROW@TU Dublin. It has been accepted for inclusion in Articles by an authorized administrator of ARROW@TU Dublin. For more information, please contact arrow.admin@tudublin.ie, aisling.coyne@tudublin.ie.



This work is licensed under a [Creative Commons Attribution-Noncommercial-Share Alike 4.0 License](#)
Funder: Irish Government Department of Agriculture, Fisheries and Food under the Food Institutional Research Measure (FIRM).

Authors

Eburne Gaston, Jesus Maria Frias, Patrick Cullen, Colm O'Donnell, and Aoife Gowen

1 **Visible Near-Infrared Hyperspectral Imaging for the Identification and**
2 **Discrimination of Brown Blotch Disease on Mushroom (*Agaricus bisporus*)**
3 **Caps**

EDURNE GASTON¹, JESÚS M. FRÍAS^{1*}, PATRICK J. CULLEN¹, COLM P. O'DONNELL² and AOIFE A. GOWEN².

¹School of Food Science and Environmental Health, Dublin Institute of Technology, Cathal Brugha Street, Dublin 1, Ireland.

²Biosystems Engineering, School of Agriculture, Food Science and Veterinary Medicine, University College Dublin, Dublin 4, Ireland.

*Corresponding author. E-mail: Jesus.Frias@dit.ie

4 **Abstract**

5 Brown blotch, caused by pathogenic *Pseudomonas tolaasii* (*P. tolaasii*), is the most
6 problematic bacterial disease in *Agaricus bisporus* mushrooms. Although it does not cause
7 any health problems, it reduces the consumer appeal of mushrooms in the market place,
8 generating important economical losses worldwide. Hyperspectral imaging (HSI) is a non-
9 destructive technique that combines imaging and spectroscopy to obtain information from a
10 sample. The objective of this study was to investigate the use of HSI for brown blotch
11 identification and discrimination from mechanical damage on mushrooms. Hyperspectral
12 images of mushrooms subjected to i) no treatment, ii) mechanical damage or iii)
13 microbiological spoilage were taken during storage and spectra representing each of the
14 classes were selected. Partial least squares- discriminant analysis (PLS-DA) was carried out
15 in two steps: i) discrimination between undamaged and damaged mushrooms and ii)
16 discrimination between damage sources (i.e. mechanical or microbiological). The models
17 were applied at a pixel level and a decision tree was used to classify mushrooms into one of
18 the aforementioned classes. A correct classification of >95% was achieved. Results from this
19 study could be used for the development of a sensor to detect and classify mushroom damage
20 of mechanical and microbial origin, which would facilitate the industry to make rapid and
21 automated decisions to discard produce of poor marketability.

22

23 **Keywords:** mushrooms, *Agaricus bisporus*, brown blotch, *Pseudomonas tolaasii*, mechanical
24 damage, vis-NIR hyperspectral imaging, PLS-DA.

25 **Introduction**

26 Cultivated mushrooms are susceptible to a variety of pests and diseases. *Pseudomonas*
27 *tolaasii* (*P. tolaasii*) is the causal agent of brown blotch (also known as bacterial blotch)
28 disease¹ and the most important pathogenic bacterium of *Agaricus bisporus*². This disease has
29 been detected and described worldwide and affects not only the button mushroom market but
30 the mushroom market in general³. According to growers, brown blotch is “the worst disease”,
31 because of the large economic losses associated to it. Brown blotch can cause a general loss
32 of crop yield of 10 % and a decrease in quality of another 10 %⁴. The most typical symptoms
33 of brown blotch are pitting and browning of mushroom tissues, induced by the watersoluble
34 toxin tolaasin⁵. This extracellular toxin is produced by the pathogenic form of *P. tolaasii*⁶.
35 The colonisation of mushroom caps by *P. tolaasii* results in the appearance of unappealing
36 brown spots on the mushroom cap and stipe³. Lesions are slightly concave blemishes,
37 sometimes small, round or spreading in many directions⁷. When the damage is more intense,
38 the spots are darker and sunken. Browning affects only the external layers of the cap tissue
39 and is restricted to 2-3 mm below the surface of the cap.

40 The mushroom industry is in need of objective evaluation methodologies to ensure that only
41 high quality produce reaches the market⁸. Studies in the field of brown blotch detection
42 include the work of Vízhányó and Felföldi⁹, who tested the potential of a machine vision
43 system to recognise and identify brown blotch and ginger blotch diseases, both of which
44 cause discolouration in mushroom caps. A vectorial normalisation method was developed to
45 decrease the effect of the natural loss of whiteness of the mushroom surface and increase the
46 differences in the image caused by the disease. The method showed an ability to discriminate
47 between discolouration caused by microbial disease and other sources of discolouration, such
48 as natural senescence. However, no attempt was made to discriminate brown blotch from

49 bruises induced by mechanical stress, which is also an important source of discolouration and
50 quality loss in the mushroom industry¹⁰.

51 Hyperspectral imaging (HSI) is a rapid and non-destructive technology that has recently
52 emerged as a powerful alternative to conventional imaging for food analysis¹¹. Hyperspectral
53 images are composed of hundreds of contiguous wavebands for each spatial position of an
54 object. Consequently, each pixel in a hyperspectral image contains the spectrum of that
55 specific position. Hyperspectral images, known as *hypercubes*, are three-dimensional blocks
56 of data, comprising two spatial and one wavelength dimension. The large quantities of highly
57 correlated data contained in a hypercube are well suited to analysis by dimension reduction
58 approaches such as principal components analysis (PCA) and partial least squares-
59 discriminant analysis (PLS-DA)¹². PLS-DA can also be applied to develop qualitative models
60 for supervised classification between various sample classes.

61 HSI has been applied at various levels in the assessment of safety and quality of food,
62 including constituent analysis¹³⁻¹⁵, quality evaluation^{16, 17} and detection of contaminants^{18, 19}
63 and defects²⁰. Additionally, a number of researchers have reported the potential of HSI for
64 identification of microorganisms of concern in food^{21, 22}. In the field of mushrooms, HSI has
65 proved useful for the detection of bruise²³ and freeze²⁴ damage and the prediction of moisture
66 content²⁵ and enzyme activity²⁶, as well as for the evaluation of shelf-life²⁷ and quality
67 deterioration²⁸. Recent advances in the detection of skin damage of other products include
68 work by Ariana et al.²⁹ with cucumbers and Nicolai et al.³⁰ and ElMasry et al.³¹ with apples.
69 As regards damage of microbial origin, Gómez-Sanchis et al.³² proposed a hyperspectral
70 imaging system for the early detection of rot caused by *Penicillium digitatum* (fungi) in
71 mandarins. This method's success in classifying rotten fruit was above 91% and it
72 represented an alternative to the operationally inefficient sorting system previously used in
73 the citrus industry. While evidence from the literature points to its feasibility, to the authors'

74 knowledge, HSI has not been used to detect damage of bacterial origin in horticultural
75 products.

76 The objective of this study was to investigate the potential application of Vis-NIR HSI for
77 brown blotch identification on mushroom caps and for its discrimination from mechanical
78 damage injuries.

79

80 **Materials and methods**

81 **Mushroom supply and damage**

82 *Agaricus bisporus* mushrooms (strain Sylvan A15, Sylvan Spawn Ltd., Peterborough, UK)
83 were grown in plastic bags and tunnels in Kinsealy Teagasc Research Centre (Kinsealy, Co.
84 Dublin, Ireland) following common practice in the mushroom industry. Only uniform
85 undamaged closed cap mushrooms from the 1st and 2nd flush with a diameter of 3-5 cm were
86 hand-picked in November 2008 (training set) and July 2009 (test set). Samples were placed in
87 a metal grid and carefully delivered to the laboratory in purpose-built containers, to minimise
88 mechanical damage during transport. Mushrooms arrived at the laboratory premises within 1
89 hour after harvesting and were stored overnight at 4°C.

90 For each set of mushrooms ($n_{\text{train}} = 144$ and $n_{\text{test}} = 108$), samples were divided in 3 groups
91 (undamaged (U), mechanically damaged (MD) and *P. tolaasii* inoculated mushroom (PT)) of
92 equal size ($n_{\text{train},i} = 48$ and $n_{\text{test},i} = 36$, where $i = \text{U, MD, PT}$).

93 Each mushroom class was treated as follows:

94 U: No treatment.

95 MD: samples were subjected to vibrational bruising to simulate crop handling and
96 transport. Mushrooms were damaged in batches of 600g (approx) units inside polystyrene
97 plastic boxes. Mechanical damage was induced by using a Gyrotory Shaker Model G2

98 shaking table (New Brunswick scientific Co., Edison, N.J., USA) at 300 rpm amplitude for a
99 shaking period of 10 min. Samples were stored in an environmental incubator (MLR-350 HT,
100 SANYO Electric Biomedical Co. Ltd., Japan) at 25°C and 90 % relative humidity (RH) for
101 24 h prior to imaging.

102 PT: samples were obtained by inoculating 4 drops of 10 µL/each of a solution of
103 pathogenic *P. tolaasii* onto each clean cap at 4×10^6 cfu. Samples were stored in the
104 incubator for 48 h at 25°C and 90 % RH prior to imaging, to encourage appearance of brown
105 blotch symptoms on the mushroom caps.

106 A total number of 252 mushrooms were used in this experiment.

107 Pathogenic *P. tolaasii* solution

108 Freeze-dried culture (DMS no. 19342) was purchased from Deutsche Sammlung von
109 Mikroorganismen und Zellkulturen GmbH (DSMZ), Germany, resuspended in nutrient broth
110 (NB, Scharlau, Dublin) and incubated at 25°C for 24 h. The pure culture was transferred into
111 nutrient agar plates (NA, Oxoid, Dublin) and incubated at optimal conditions to obtain
112 isolated colonies.

113 “Mushroom tissue block rapid pitting” and “White Line in Agar” (WLA) pathogenicity tests
114 were carried out following the procedure of Wong and Preece³³ to confirm culture
115 pathogenicity on mushrooms.

116 - *Mushroom tissue block rapid pitting test*

117 The outer skin of a mushroom was peeled off and mushroom cap tissue blocks of approx.
118 $15 \times 15 \times 5$ mm were cut. Bacterial isolates were grown on Pseudomonas agar base
119 (PAB, Oxoid, Dublin) at 25°C for 24 h and suspended in sterile distilled water (10^8 cfu
120 mL⁻¹ approx). Mushroom blocks were placed in duplicate on Petri dishes containing
121 sterile water-moistened filter paper. The bacterial solution was inoculated onto the cut

122 surface of one of the mushroom blocks and incubated at 25°C. Sterile water was
123 inoculated onto the surface of the other mushroom blocks for negative control. Pitting of
124 the cut surface of mushroom tissue revealed pathogenicity of *P. tolaasii* on the mushroom
125 blocks.

126 *“White Line in Agar” test*

127 *Pseudomonas reactans* (*P. reactans*) was streaked out in a line, directly from agar slope
128 culture, across PAB in a Petri dish. This strain had been isolated and provided by
129 Kinsealy Teagasc Research Centre.

130 The *P. tolaasii* isolate to be tested was streaked immediately after on to the plates at right
131 angles to the reacting organism (i.e. *P. reactans*). Plates were incubated at 25°C for 24 h
132 for the production of a white line with the reacting organism.

133 White line production in the agar between *P. reactans* and *P. tolaasii* was interpreted as
134 positive interaction between colonies and a positive response for pathogenicity test.

135 A loopfull of pathogenicity confirmed working culture was transferred to a sterile 0.8% saline
136 solution (Sigma, Dublin). 4 droplets of 10 µL/each of a 10⁸ cfu mL⁻¹ solution were inoculated
137 onto the cap, resulting in inoculation concentration of 4 × 10⁶ cfu.

138 **Hyperspectral imaging**

139 Hyperspectral images were obtained using a pushbroom line-scanning HSI instrument (DV
140 Optics Ltd, Padua, Italy). The instrument comprised a moving table, illumination source (150
141 W halogen lamp source attached to a fibre optic line light positioned parallel to the moving
142 table), mirror, objective lens (25 mm focal length), Specim V10E spectrograph (Spectral
143 Imaging Ltd, Oulu, Finland) operating in the wavelength range of 400-1000 nm
144 (spectroscopic resolution of 5 nm), CCD camera (Basler A312f, effective resolution of 580 ×
145 580 pixels by 12 bits), acquisition software (SpectralScanner, DV Optics, Padua, Italy) and

146 PC. A cylindrical diffuser was placed in front of the fibre optic line light to produce a diffuse
147 light source. In this study, only spectral data within the wavelength range of 445-945 nm
148 were used, as beyond this range the noise level of the camera was high and the signal
149 efficiency of the light source was low.

150 Reflectance calibration

151 Reflectance calibration was carried out prior to mushroom image acquisition in order to
152 account for the background spectral response of the instrument and the “dark” camera
153 response. The bright response (“*W*”) was obtained by collecting a hypercube from a uniform
154 white ceramic tile; the dark response (“*dark*”) was acquired by turning off the light source,
155 completely covering the lens with its cap and recording the camera response. The corrected
156 reflectance value (“*R*”) was calculated from the measured signal (“*I*”) on a pixel-by-pixel
157 basis as shown by:

$$158 \quad R_i = \frac{(I_i - dark_i)}{(W_i - dark_i)}$$

159 where *i* is the pixel index, i.e. $i=1,2,3,\dots,n$ and *n* is the total number of pixels.

160 HSI images of U mushrooms were acquired on day 0 of the experiment. MD mushrooms
161 were scanned after 24 h of storage. PT mushroom images were taken after 48 h of storage.

162 Data were recorded in units of reflectance and saved in ENVI header format using the
163 acquisition software.

164 **Confirmation of *P. tolaasii***

165 After image acquisition of PT mushrooms on day 2 of storage, 0.5 g of the outer skin of 10 %
166 of each mushroom class were extracted with a sharp sterile knife. Skins were suspended
167 separately in 10 mL of a 0.8 % saline solution. Samples were homogenised in a stomacher

168 (Seward BA 7020, Seward, UK) for 60 s at high intensity. Serial dilutions of each suspension
169 were prepared and transferred onto NA and PAB plates, which were incubated for 48 h at
170 25°C to obtain isolated colonies. The same procedure had been carried out after image
171 acquisition of U mushrooms on day 0 and resulting colonies were used as negative controls.
172 Serial dilutions of the pathogenic *P. tolaasii* solution that had been used to inoculate PT
173 mushrooms were also prepared and transferred onto NA and PAB plates; resulting colonies
174 were used as positive controls.

175 Mushroom tissue block rapid pitting and WLA tests were carried out to test for pathogenicity
176 of isolated colonies.

177 **Image processing**

178 For each mushroom hyperspectral image, 175 characteristic (i.e. U, MD or PT, depending on
179 mushroom class) regions of interest (ROI) were selected by using an interactive selection tool
180 (“*ROI tool*”) available in the acquisition software. The ROI’s were 3 × 3 pixels in size and
181 were selected from the central region of the mushroom cap, where possible. Selecting spectra
182 from analogous surface areas in all the mushrooms aimed at minimising the scaling
183 differences caused by mushroom surface curvature²⁴. The average reflectance spectrum (“*R*”)
184 of each ROI was obtained by averaging the pixel spectra of the region. Spectral data of each
185 mushroom set were used to build two-dimensional matrices, where each row represented the
186 spectrum of one ROI.

187 Prior to the development of multivariate models for damage class prediction, spectra were
188 pre-processed using the Standard Normal Variate (SNV) transformation to reduce spectral
189 variability due to non-chemical biases³⁴.

190 Training set matrices (raw and SNV-corrected) contained 8400 spectra and test set matrices
191 (raw and SNV) contained 6300 spectra.

192 **Partial least squares- discriminant analysis (PLS-DA)**

193 Partial least-squares discriminant analysis was applied to the training set matrices (raw and
194 SNV-corrected, n=8400) using MATLAB 7.0 (The Math Works, Inc. USA). The aim was to
195 build models that would enable maximum separation of sample spectra into different classes
196 depending on their physical condition. A two step model approach was taken for each set of
197 spectra (i.e. raw and SNV): one model (namely “U/Dam” model) was developed to
198 discriminate between undamaged (U) and damaged (Dam) spectra and another model
199 (namely “MD/PT” model) was built to discriminate between the two classes of Dam, i.e.
200 mechanical (MD) and microbiological (PT). Overall, four models were built: U/Dam_raw,
201 U/Dam_SNV, MD/PT_raw and MD/PT_SNV.

202 For this purpose, a dummy response variable, Y , was constructed and assigned to each
203 spectrum. For U/Dam models, $Y = 0$ for U spectra and $Y = 1$ for Dam spectra. For MD/PT
204 models, $Y = 0$ for MD spectra and $Y = 1$ for PT spectra. In both cases, a cut-off value of 0.5
205 was used to classify spectra, as suggested by Esquerre, Gowen, O'Donnell & Downey³⁵;
206 spectra with a predicted dummy variable <0.5 were identified as belonging to class 0, while
207 those with predicted Y -value ≥ 0.5 were classified as belonging to class 1.

208 Spectra from the training data set were split into 10 sections and continuous blocks cross-
209 validation was performed. The decision on the number of latent variables (# LV) to select for
210 each model was made based on the root-mean square error of cross-validation (RMSECV),
211 which is the mean of the sum of squared differences between the actual and the predicted
212 value of the dummy variable.

213 The models were also applied to the test set matrices (raw and SNV-corrected, n=6300),
214 which represented independent sets of sample spectra. Performance of the classification
215 models was evaluated on the basis of their sensitivity (number of spectra of a given type

216 correctly classified as that type) and specificity (number of spectra not of a given type
217 correctly classified as not of that type) on training and test sets.

218 **Prediction maps**

219 An important feature of hyperspectral imaging is the ability to map the distribution of
220 components/attributes on samples. In this case, developed PLS-DA models could be applied
221 to entire hypercubes of mushrooms to form two dimensional prediction images where the
222 damage class of each pixel as predicted by the PLS-DA models would be represented by its
223 intensity (“*I*”). With this in mind, the following step-by-step procedure was carried out on all
224 mushroom hypercubes:

- 225 1. Masking. This step was performed to separate the mushroom pixels from the
226 background. The mask was created by thresholding the mushroom image at 940 nm,
227 where a pixel threshold value of 0.1 was used to segment the mushroom from the
228 background. All background regions were set to zero and only the non-zero elements
229 of the image were used in further steps.
- 230 2. Erosion. As all the spectra collected to build the models corresponded to interactively
231 selected ROI’s of the central part of the mushrooms, the image outline (i.e. edge) of
232 the mushrooms was eroded to spectra showing differences due to sample curvature.
233 This was done by eroding the masks using disk-shaped structuring elements (SE,
234 whose radii increased from 0 –i.e. no erosion- to 40 pixels, in 10 pixel gaps), prior to
235 the application of PLS-DA models. The effect that varying the radius of the SE had on
236 i) the area of the mask, ii) the pixel distribution of the predicted maps and iii) the
237 performance statistics of the two models at a pixel level, based upon ANOVA results
238 obtained using R^{36} , was studied.

- 239 3. Application of developed PLS-DA models. The U/Dam model was applied to eroded
240 hypercubes and following this classification, the MD/PT model was applied only to
241 the pixels previously classified as *Dam*. Three binary images (Bin_U , Bin_{MD} and Bin_{PT} ,
242 one for each damage class, where 1 indicated class membership and 0 indicated non-
243 membership) were generated after classifying each pixel as “*U*” ($I_{U/Dam} < 0.5$), “*MD*”
244 ($I_{U/Dam} > 0.5$ and $I_{MD/PT} < 0.5$) or “*PT*” ($I_{U/PT} > 0.5$ and $I_{MD/PT} > 0.5$) tissue.
- 245 4. Closing. As enzymatic browning was expected to develop uniformly across MD
246 mushroom caps and bacterial lesions were expected to appear as brown spots of
247 visible size, Bin_{MD} images *closed*³⁷ in order to avoid noise in the form of isolated *PT*
248 pixels in such maps. The *Closing* morphological operator performs dilation followed
249 by erosion; this was done using a diamond-shaped SE with a radius of 3 pixels. The
250 effect of omitting/incorporating Step 4 on i) the pixel distribution of the prediction
251 maps and ii) performance statistics, based upon ANOVA results, was investigated.
- 252 5. Concatenation: the three binary maps (i.e. Bin_U , Bin_{MD} and Bin_{PT}) were concatenated
253 to build false colour maps where *U*, *MD* and *PT* classified pixels were represented in
254 green, red and blue, respectively.

255 **Mushroom classification**

256 Based on the percentage of pixels of each damage class on the prediction map, a decision tree
257 (shown in Figure 1) was used to allocate each mushroom to one of the three mushroom
258 classes. As the main objective of this work was to identify *P. tolaasii* inoculated mushrooms,
259 the *PT* pixel percentage of the prediction maps was selected as the discrimination criteria and
260 a cut-off value was established by exploring the pixel histograms of the Bin_{PT} images of U,
261 MD and PT mushrooms (Figure 2). A *PT* pixel percentage of 2 % appeared to be a reasonable
262 cut-off point, as all of the U mushroom predictions and almost all of the MD mushroom
263 predictions exhibited lower values and almost all of the PT mushroom predictions showed

264 higher values. After visual inspection of the two PT mushrooms that were below the cut-off
265 value, it was observed that these two mushrooms did not develop any brown blotch on their
266 caps, for which they could be left out for cut-off establishment purposes. As it can be seen in
267 the figure, when the number of *PT* pixels in the prediction image was higher than 2 %, the
268 mushroom was classified as PT. If the number of *PT* pixels was lower than 2 % and the
269 amount of *MD* pixels was higher than the amount of *U* pixels, the mushroom was classified
270 as MD. Finally, if the number of *PT* pixels was lower than 2 % and the amount of *MD* pixels
271 was lower than the amount of *U* pixels, the mushroom was classified as U.

272 Sensitivity and specificity of the classification procedure were computed after the application
273 of the decision tree to all of the mushroom hypercubes.

274 **Results and discussion**

275 **RGB images**

276 Figure 3 shows representative colour images of the three mushroom classes under
277 investigation in this study. Mushrooms labelled as U (Figure 3a) were white in general
278 appearance, although some of them showed some signs of natural discolouration caused by
279 common picking and transport practice. By day one of storage, MD samples (Figure 3b)
280 exhibited uniform browning over the entire mushroom surface. By day two of storage, *P.*
281 *tolaasii* had colonised the cap of most PT mushrooms (Figure 3c), which exhibited slightly
282 concave brown-coloured spots, the typical symptoms of brown blotch disease.

283 **Confirmation of *P. tolaasii***

284 The prevalence of *Pseudomonas* in mushroom surfaces is high, but only pathogenic *P.*
285 *tolaasii* is capable of causing brown blotch. Two different types of colonies, whose colours
286 were a) creamy and b) green, were found in PAB plates of PT mushrooms, while only one
287 type appeared in PAB plates of U mushrooms and the *P. tolaasii* inoculum; the colour of

288 these colonies was creamy and green, respectively. Isolates of the two types found in PT
289 mushroom plates were obtained by re-streaking representative colonies onto fresh PAB
290 plates. Figure 4 shows growth in PAB plates of the two types of colonies of PT mushrooms
291 (Figures 4a, creamy colonies and 4b, green), the creamy colonies of U mushrooms (Figure
292 4c) and the green colonies of the *P. tolaasii* inoculum (Figure 4d). The creamy colonies of PT
293 mushrooms (Figure 4a) were found to be similar to those found in U plates (Figure 4c), and
294 both gave a negative response to the mushroom tissue block rapid pitting and WLA tests. The
295 green colonies of PT mushrooms (Figure 4b) were similar to those found in *P. tolaasii*
296 inoculum plates (Figure 4d) and both had a positive response to the two pathogenicity tests.
297 These results confirm that the pitting observed in PT mushrooms was due to pathogenic *P.*
298 *tolasii*.

299 **Spectra**

300 Mean spectra of the various spectra classes are shown in Figure 5: (a) non-pretreated
301 reflectance spectra and (b) SNV-corrected reflectance spectra. In Figure 5a, signal intensity
302 and shape differences between U and MD spectra were remarkable. The mean MD spectrum
303 exhibited lower reflectance values over the entire spectral region, as expected after bruising
304 had led to loss of whiteness of the caps. The greatest differences in shape between MD and U
305 spectra arose in the 600-800 nm region, where the mean U spectrum exhibited broader
306 features than the mean MD spectrum. Broad spectra in the visible-near infrared wavelength
307 range are characteristic of undamaged mushrooms, corresponding to their white appearance.
308 The spectral differences mentioned above could be related to the formation of brown
309 pigments, mainly melanins, which derive from enzyme-catalysed oxidation products called
310 quinones. The mean PT spectrum appeared to be more similar in shape to the mean MD
311 spectrum, although its slope was not as linear as MD's was in the 600-800 nm region.

312 Spectral differences in Figure 5a arose from differences in sample composition, but
313 differences in illumination conditions, sample height and curvature may also have affected
314 the spectral response of the different mushroom classes. Spectra preprocessing methods such
315 as Multiplicative Scatter Correction (MSC)³⁸ and SNV³⁴ can be used to compensate for
316 spectral variability caused by these external factors³⁹.

317 The mean spectra of SNV-corrected reflectance spectra of U, MD and PT spectra are shown
318 in Figure 5b. Comparing U and MD spectra, MD exhibited higher SNV-corrected reflectance
319 values in the 450-500 nm region and lower SNV-corrected reflectance in the 500-750 nm
320 region. The oxidation of polyphenolic compounds and subsequent development of brown
321 colour in the MD mushrooms might be partly responsible for this dissimilarity³⁵. In the 800-
322 950 nm region, MD spectra showed higher values than U mushrooms. Overall, the shape of
323 the mean spectrum of PT spectra was somewhat intermediate between the mean of U and MD
324 spectra in the wavelength range of study. The visible end of the mean PT spectrum looked
325 more similar to MD than to U, whereas its shape in the >700 nm region was very similar to
326 that of U mushrooms’.

327 **PLS-DA analysis**

328 Figure 6 shows RMSECV and performance statistics (i.e. sensitivity and specificity) of the
329 four PLS-DA models developed, as a function of the number of latent variables (from 1 to
330 10). In binary classifications, the sensitivity of a model is a measure of its ability to correctly
331 classify spectra of a given type as being of that type, whereas the specificity is a measure of
332 its ability to correctly classify spectra which are not of a given type as not being of that type.
333 For both U/Dam models (Figs. 6a and 6b), RMSECV exhibited a “corner” (pointed with a red
334 dash circle) at 2 LV. The performance statistics, which were very poor at 1LV, increased at
335 that point and remained at similar levels thereafter, for which 2 was considered to be the
336 optimal # LV for models discriminating between U and Dam spectra. Both MD/PT models

337 seemed to perform best when 4 LV were selected; RMSECV did not decrease significantly
338 after that and performance statistics remained high.

339 Numeric values of performance statistics of the selected models are shown in Table 1. When
340 the models built with raw spectra were applied to the training set of spectra, almost perfect
341 classification was achieved in the case of the U/Dam model (sensitivity = 0.997 and
342 specificity = 1.000). The model performed worse when built on SNV-corrected spectra
343 (sensitivity = 0.973 and specificity = 0.999); however differences in sensitivity and
344 specificity were very small. In both cases, almost all of the Dam spectra were classified as
345 such and none or only a few U were misclassified as Dam. When the MD/PT model was
346 applied to the damaged spectra, the sensitivity of the raw model (sensitivity = 0.988) was
347 higher than that of the SNV-corrected model (sensitivity = 0.963), whereas the specificity of
348 the MD/PT_raw model was lower than the MD/PT_SNV model's (0.983 and 0.998,
349 respectively). These results showed that almost all of the spectra of the mushrooms that had
350 been inoculated with *P. tolaasii* were classified correctly and only a few or none of the
351 spectra of the MD samples were misclassified as PT.

352 When the models were applied to the test set of spectra, the sensitivity of the U/Dam_raw
353 model was lower (sensitivity = 0.832) but still none of the U spectra were misclassified as
354 Dam (specificity = 1.000). Performance statistics were quite similar for the U/Dam_SNV
355 model (sensitivity = 0.825 and specificity = 0.999). When the MD/PT model was applied to
356 the damaged spectra of the test set, a smaller percentage of raw PT spectra were classified
357 correctly (sensitivity = 0.661) but almost none of the MD spectra were misclassified as PT
358 (specificity = 0.984). As observed for the previous model, the sensitivity of the MD/PT_SNV
359 model was slightly lower (sensitivity = 0.641) and the specificity was higher (specificity =
360 0.998).

361 Overall, models built on raw reflectance spectra performed better in this study. However,
362 with a view to generalising the use of U/Dam and MD/PT discrimination models, it might be
363 worthwhile to compromise classification performance in favour of employing more versatile
364 models (e.g. models built on SNV-corrected spectra).

365 **Prediction maps**

366 Figure 7 shows examples of prediction maps (with no erosion applied in Step 2) of (a) U, (b)
367 MD and (c) PT mushrooms as a result of the application of raw (top row) and SNV-corrected
368 (bottom row) PLS-DA models to the data hypercubes. Overall, predictions by models built on
369 raw reflectance spectra appeared to be more appropriate than predictions by models built on
370 SNV-corrected reflectance spectra: for each mushroom class, the corresponding pixel class
371 was the main pixel class and pixels were distributed in an even manner. In the example
372 shown (Figure 7), on the top row (i.e. predictions by models built on raw reflectance spectra),
373 neither the map of the U mushroom nor the central region of the prediction of the MD
374 mushroom showed misclassification, whereas most edge pixels of the latter were
375 misclassified as U. Considering that all the spectra selected for model building belonged to
376 central regions of the mushrooms, this misclassification could be related to the inability of the
377 models to account for spectral differences due to mushroom surface curvature. Fewer pixels
378 were misclassified in the prediction map of the PT mushroom, where some pixels were
379 classified as MD. On the bottom row of Figure 7 (i.e. prediction maps by models built on
380 SNV-corrected reflectance spectra), the maps of all mushroom types showed
381 misclassification. For U and PT mushrooms, misclassification happened mainly but not only
382 on the edges, where many U pixels were classified as MD. For MD mushrooms, misclassified
383 pixels were distributed evenly along the mushroom surface. In this case, MD pixels were
384 misclassified as PT.

385 Considering that the main focus of this work lies in the identification of PT mushrooms, after
386 visual inspection of the prediction maps (Figure 7), PLS-DA models built on non-pretreated
387 spectra were considered more appropriate for this purpose. Models built on SNV-corrected
388 reflectance spectra were therefore discarded and further sections of this paper will focus only
389 on models built on the raw data.

390 Effect of varying the radius of the SE in Step 2

391 Erosion of a binary image is a basic operation to wear the boundaries of regions away. This
392 can be done to overcome the problem introduced by the so-called “edge effect”, by which
393 variability in reflection of light is introduced by spherical surfaces⁴⁰. In this particular case,
394 where PLS-DA models were built on spectra selected from central regions of the mushrooms,
395 it was expected that these models would perform better on central areas of the mushrooms
396 than on edge regions. For this reason, masks defining the mushroom region were eroded
397 using SE’s before the models were applied (see Step 2 in *Prediction maps* section). This led
398 to a decrease in misclassified pixels (typically belonging to edge regions, as observed in
399 Figure 7b, top row).

400 Figure 8a shows the effect that increasing the size of the structuring element used in this step
401 (i.e. Step 2) had on the mask (top row) and on the prediction map (bottom row) of a MD class
402 mushroom. As the radius increased (from left to right, from 0 -no erosion- to 40 pixels), the
403 mask became smaller. Consequently, the number of MD class pixels that were misclassified
404 (as U class) decreased progressively. Figure 8b shows the decrease of the average relative
405 area of the mushroom region as a function of the radius of SE, where the relative area of each
406 mask at a certain SE radius value is displayed as a percentage of the area of the mask when
407 the radius was zero (i.e. when no erosion was applied) and the average and standard deviation
408 values were obtained by considering all the mushrooms in the training and test data sets.
409 Figure 8c shows the sensitivity of the PLS-DA models built on raw reflectance spectra

410 applied at a pixel level as a function of the radius of the SE. The sensitivity of the U/Dam
411 model reached its maximum (sensitivity = 1) at a radius value of 20 pixels when applied to
412 the training set and at a radius value of 40 (sensitivity = 0.972) when applied to the test set.
413 The sensitivity of the MD/PT model was not affected by the radius and remained at its
414 maximum (sensitivity = 1) for the training set, whereas it increased progressively until it
415 reached its maximum (sensitivity = 0.944) at a radius value of 40 pixels. Modifying the
416 radius of the SE did not affect ($p>0.05$) the specificity of the PLS-DA models (results not
417 shown).

418 Effect of omitting/incorporating Step 4

419 As the existence of isolated *PT* pixels in the prediction map had no physical meaning (brown
420 blotch lesion on mushroom caps are detectable by the human eye), a *closing* step (see Step 4
421 of *Prediction maps* section) was incorporated to the prediction map routine. This step
422 performed dilation followed by erosion on the Bin_{PT} images. Figure 9a shows how the final
423 prediction of a MD class mushroom looked when i) Step 4 was omitted and ii) Step 4 was
424 incorporated in the routine. As it can be observed in the figures, Step 4 removed *PT* class
425 isolated pixels (blue) in the prediction image and converted them into pixels of class *MD*
426 (red). The effect that such conversion had on the performance statistics of the models at a
427 pixel level was studied and only the specificity of the MD/PT_raw model on the test set was
428 found to change significantly ($p<0.05$). Figure 9b shows how specificity changed as the
429 radius of the SE of Step 2 increased, when i) Step 4 was omitted (round marker) and ii) Step
430 4 was incorporated (square marker) in the routine. The specificity of the MD/PT_raw model
431 improved when this step was incorporated, which means more MD class mushrooms were
432 correctly classified. This figure suggests that adding a *closing* step was important to achieve
433 good levels of classification.

434 After studying the two effects, a disk radius of 40 pixels was selected for the SE of Step 2 and
435 it was decided to include Step 4 in the generation of prediction maps. Further sections of this
436 paper will only focus on results based on the use of the aforementioned steps.

437 **Mushroom classification**

438 The application of PLS-DA models built on raw spectra to the totality of entire hypercubes
439 led to the performance statistics shown in Table 2. For the training set mushrooms, both the
440 sensitivity and the specificity of the U/Dam_raw model were 1, which means there was no
441 misclassification at all. For the same samples, the sensitivity of the MD/PT_raw model was 1
442 and its specificity was 0.98. Only 1 out of 48 MD mushroom was misclassified as a PT
443 mushroom. The models performed quite similarly for the mushroom hypercubes of the test
444 set: for the U/Dam_raw model, sensitivity = 0.97 and specificity = 1. Only 2 out of 72 Dam
445 mushrooms were misclassified as U, and none of the U was misclassified as Dam. For the
446 MD/PT_raw model, sensitivity = 0.944 (only 2 out of 36 PT mushrooms were not classified
447 as such) and specificity = 0.97 (only 1 MD mushroom was misclassified as being PT).

448 These results show the models performed well when applied at a pixel level and could be the
449 first step towards the development of a HSI sensor that would classify independent sets of
450 mushrooms with high levels of accuracy. Overall, the correct classification of the models
451 presented in this paper is higher than the classification of the algorithms by Vízhányó and
452 Felföldi⁹, which correctly classified 81% of the diseased areas of test mushrooms using
453 conventional computer imaging. It should be noted that the procedure described in this paper
454 is longer and more complex than the one presented in that study, and the technology more
455 costly. While the algorithms presented in the aforementioned paper discriminated diseased
456 spots from healthy senescent mushroom parts, the models developed in this paper
457 discriminate microbial spoilage from both undamaged and mechanically damaged samples.

458 The correct discrimination between PT and MD mushrooms ensure no misclassification of
459 samples whose colour analysis might be similar and hence avoid “false positives”.

460 **Conclusion**

461 Results presented in this work show that raw reflectance data of mushroom caps could be
462 used to classify mushrooms according to their damage class (i.e. undamaged, mechanically
463 damaged or brown blotch diseased). PLS-DA models were developed to initially sort
464 mushrooms into undamaged or damaged classes and to further classify the damaged into
465 mechanically damaged or microbiologically diseased classes. The application of the models
466 at a pixel level together with the use of a decision tree allowed for correct classification of
467 >95%. This study demonstrates the potential use of hyperspectral imaging as an automated
468 tool for detection of brown blotched mushrooms and for their discrimination from
469 mechanically damaged mushrooms. Knowledge gained in this research using HSI could be
470 incorporated towards the development of simpler sensors to detect and classify mushroom
471 damage of different sources. Such a system could aid the industry in increasing quality
472 control standards by correctly identifying low quality produce. However, further research and
473 validation at industrial scale are required to facilitate its adoption.

474 **Acknowledgements**

475 The authors would like to thank Ted Cormican and Dr. Helen Grogan from the Teagasc
476 Research Station at Kinsealy, Dublin, for producing mushrooms and providing *Pseudomonas*
477 *reactans* strains and Dr. Paula Bourke and Dr. Patricia Nobmann from Dublin Institute of
478 Technology for kind technical advice. This research was funded by the Irish Government
479 Department of Agriculture, Fisheries and Food under the Food Institutional Research
480 Measure (FIRM).

481 **References**

- 482 1. S.G. Paine, "Studies in Bacteroiosis II: A Brown Blotch Disease of Cultivated
483 Mushrooms", *Annals of Applied Biology* **5**, [1919].
- 484 2. N.G. Nair and J.K. Bradley, "Mushroom Blotch Bacterium During Cultivation", *The*
485 *Mushroom Journal* **90**, [1980].
- 486 3. C. Soler-Rivas, S. Jolivet, N. Arpin, J.M. Olivier and H.J. Wichers, "Biochemical and
487 Physiological Aspects of Brown Blotch Disease of *Agaricus Bisporus*", *FEMS*
488 *Microbiology Reviews* **23**, [1999].
- 489 4. P.B. Rainey, C.L. Brodey and K. Johnstone, "Biology of *Pseudomonas Tolaasii*,
490 Cause of Brown Blotch Disease of the Cultivated Mushrooms", in *Advances in Plant*
491 *Pathology* **8**, Ed by J.H. Andrews and I.C. Tommerup. Academic Press, p. 95-117
492 [1992].
- 493 5. F. Moquet, M. Mamoun and J.M. Olivier, "*Pseudomonas Tolaasii* and Tolaasin:
494 Comparison of Symptom Induction on a Wide Range of *Agaricus Bisporus* Strains",
495 *FEMS Microbiology Letters* **142**, [1996].
- 496 6. J.C. Nutkins, R.J. Mortishire-Smith, L.C. Packman, C.L. Brodey, P.B. Rainey, K.
497 Johnstone and D.H. Williams, "Structure Determination of Tolaasin, an Extracellular
498 Lipodepsipeptide Produced by Mushroom Pathogen *Pesudomonas Tolaasii* Paine",
499 *Journal of American Chemical Society* **113**, [1991].
- 500 7. J.M. Olivier, J. Guillaumes and D. Martin, "Study of a Bacterial Disease of
501 Mushroom Caps", in *4th International Conference on Plant Pathogenic Bacteria*,
502 Angers, France [1978].
- 503 8. P.H. Heinemann, R. Hughes, C.T. Morrow, H.J. Sommer, R.B. Beelman and P.J.
504 Wuest, "Grading of Mushrooms Using a Machine Vision System", *Transactions of*
505 *the ASAE* **37**, 5 [1994].

- 506 9. T. Vízhányó and J. Felföldi, "Enhancing Colour Differences in Images of Diseased
507 Mushrooms", *Computers and Electronics in Agriculture* **26**, [2000].
- 508 10. S. Jolivet, N. Arpin, H.J. Wichers and G. Pellom, "*Agaricus Bisporus* Browning: A
509 Review", *Mycological Research* **102**, 12 [1998].
- 510 11. A.A. Gowen, C.P. O'Donnell, P.J. Cullen, G. Downey and J.M. Frías, "Hyperspectral
511 Imaging - an Emerging Process Analytical Tool for Food Quality and Safety Control",
512 *Trends in Food Science and Technology* **18**, [2007].
- 513 12. A.A. Gowen, C.P. O'Donnell, M. Taghizadeh, P.J. Cullen, J.M. Frias and G. Downey,
514 "Characterisation of Blemishes on White Mushroom (*Agaricus Bisporus*) Caps Using
515 Hyperspectral Imaging", in *10th International conference on Engineering and Food -*
516 *ICEF 10*, Viña del Mar, Chile [2008].
- 517 13. Y. Peng and R. Lu, "Analysis of Spatially Resolved Hyperspectral Scattering Images
518 for Assessing Apple Fruit Firmness and Soluble Solids Content", *Postharvest Biology*
519 *and Technology* **48**, 1 [2008].
- 520 14. S.T. Monteiro, Y. Minekawa, Y. Kosugi, T. Akazawa and K. Oda, "Prediction of
521 Sweetness and Amino Acid Content in Soybean Crops from Hyperspectral Imagery",
522 *ISPRS Journal of Photogrammetry and Remote Sensing* **62**, 1 [2007].
- 523 15. J. Qiao, N. Wang, M. Ngadi and S. Baljinder, "Water Content and Weight Estimation
524 for Potatoes Using Hyperspectral Imaging", in *2005 ASAE Annual Meeting, Paper*
525 *No. 053126*, St. Joseph, Michigan, USA [2005].
- 526 16. L. Liu, M.O. Ngadi, S.O. Prasher and C. Gariépy, "Categorization of Pork Quality
527 Using Gabor Filter-Based Hyperspectral Imaging Technology", *Journal of Food*
528 *Engineering* **99**, 3 [2010].
- 529 17. H.K. Noh and R. Lu, "Hyperspectral Laser-Induced Fluorescence Imaging for
530 Assessing Apple Fruit Quality", *Postharvest Biology and Technology* **43**, 2 [2007].

- 531 18. B. Park, K.C. Lawrence, W.R. Windham and D.P. Smith, "Performance of
532 Hyperspectral Imaging System for Poultry Surface Fecal Contaminant Detection",
533 *Journal of Food Engineering* **75**, 3 [2006].
- 534 19. Y. Liu, Y.-R. Chen, M.S. Kim, D.E. Chan and A.M. Lefcourt, "Development of
535 Simple Algorithms for the Detection of Fecal Contaminants on Apples from
536 Visible/near Infrared Hyperspectral Reflectance Imaging", *Journal of Food*
537 *Engineering* **81**, 2 [2007].
- 538 20. D.P. Ariana and R. Lu, "Evaluation of Internal Defect and Surface Color of Whole
539 Pickles Using Hyperspectral Imaging", *Journal of Food Engineering* **96**, 4 [2010].
- 540 21. J. Dubois, E. Neil Lewis, J.F.S. Fry and E.M. Calvey, "Bacterial Identification by
541 near-Infrared Chemical Imaging of Food-Specific Cards", *Food Microbiology* **22**, 6
542 [2005].
- 543 22. M.F. Escoriza, J.M. VanBriesen, S. Stewart, J. Maier and P.J. Treado, "Raman
544 Spectroscopy and Chemical Imaging for Quantification of Filtered Waterborne
545 Bacteria", *Journal of Microbiological Methods* **66**, 1 [2006].
- 546 23. A.A. Gowen, C.P. O'Donnell, M. Taghizadeh, P.J. Cullen and G. Downey,
547 "Hyperspectral Imaging Combined with Principal Component Analysis for Bruise
548 Damage Detection on White Mushrooms (*Agaricus Bisporus*)", *Journal of*
549 *Chemometrics* **22**, 3-4 [2008].
- 550 24. A.A. Gowen, M. Taghizadeh and C.P. O'Donnell, "Identification of Mushrooms
551 Subjected to Freeze Damage Using Hyperspectral Imaging", *Journal of Food*
552 *Engineering* **93**, 1 [2009].
- 553 25. M. Taghizadeh, A. Gowen and C.P. O'Donnell, "Prediction of White Button
554 Mushroom (*Agaricus Bisporus*) Moisture Content Using Hyperspectral Imaging",
555 *Sensing and Instrumentation for Food Quality and Safety* **4**, [2009].

- 556 26. E. Gaston, J.M. Frías, P.J. Cullen, C.P. O'Donnell and A.A. Gowen, "Prediction of
557 Polyphenol Oxidase Activity Using Visible near-Infrared Hyperspectral Imaging on
558 Mushroom (*Agaricus Bisporus*) Caps", *Journal of Agricultural and Food Chemistry*,
559 doi: 10.1021/jf00501q.
- 560 27. M. Taghizadeh, A. Gowen and C.P. O'Donnell, "Use of Hyperspectral Imaging for
561 Evaluation of the Shelf-Life of Fresh White Button Mushrooms (*Agaricus Bisporus*)
562 Stored in Different Packaging Films", *Innovative Food Science and Emerging
563 Technologies*, doi: 10.1016/j.ifset.2010.01.016.
- 564 28. A.A. Gowen, C.P. O'Donnell, M. Taghizadeh, E. Gaston, A. O'Gorman, P.J. Cullen,
565 J.M. Frías, C. Esquerre and G. Downey, "Hyperspectral Imaging for the Investigation
566 of Quality Deterioration in Sliced Mushrooms (*Agaricus Bisporus*) During Storage",
567 *Sensing and Instrumentation for Food Quality and Safety* **2**, 3 [2008].
- 568 29. D.P. Ariana, R. Lu and D.E. Guyer, "Near-Infrared Hyperspectral Reflectance
569 Imaging for Detection of Bruises on Pickling Cucumbers", *Computers and
570 Electronics in Agriculture* **53**, 1 [2006].
- 571 30. B.M. Nicolai, E. Lötze, A. Peirs, N. Scheerlinck and K.I. Theron, "Non-Destructive
572 Measurement of Bitter Pit in Apple Fruit Using Nir Hyperspectral Imaging",
573 *Postharvest Biology and Technology* **40**, 1 [2006].
- 574 31. G. ElMasry, N. Wang and C. Vigneault, "Detecting Chilling Injury in Red Delicious
575 Apple Using Hyperspectral Imaging and Neural Networks", *Postharvest Biology and
576 Technology* **52**, 1 [2009].
- 577 32. J. Gómez-Sanchis, L. Gómez-Chova, N. Aleixos, G. Camps-Valls, C. Montesinos-
578 Herrero, E. Moltó and J. Blasco, "Hyperspectral System for Early Detection of
579 Rottenness Caused by *Penicillium Digitatum* in Mandarins", *Journal of Food
580 Engineering* **89**, 1 [2008].

- 581 33. W.C. Wong and T.F. Preece, "Identification of *Pseudomonas Tolaasii* : The White
582 Line in Agar and Mushroom Tissue Block Rapid Pitting Tests", *Journal of Applied*
583 *Bacteriology* **47**, [1979].
- 584 34. R.J. Barnes, M.S. Dhanoa and S.J. Lister, "Standard Normal Variate Transformation
585 and Detrending of near Infrared Diffuse Reflectance Spectroscopy", *Applied*
586 *Spectroscopy* **43**, 5 [1989].
- 587 35. C. Esquerre, A.A. Gowen, C.P. O'Donnell and G. Downey, "Initial Studies on the
588 Quantitation of Bruise Damage and Freshness in Mushrooms Using Visible-near-
589 Infrared Spectroscopy", *Journal of Agricultural and Food Chemistry* **57**, [2009].
- 590 36. R_Development_Core_Team, *R: A Language and Environment for Statistical*
591 *Computing*. R Foundation for Statistical Computing, Vienna, Austria [2007].
- 592 37. A. Rocha, D.C. Hauagge, J. Wainer and S. Goldenstein, "Automatic Fruit and
593 Vegetable Classification from Images", *Computers and Electronics in Agriculture* **70**,
594 1 [2010].
- 595 38. P. Geladi, D. MacDougall and H. Martens, "Linearization and Scatter-Correction for
596 near-Infrared Reflectance Spectra of Meat", *Applied Spectroscopy* **39**, 3 [1985].
- 597 39. T. Azzouz, A. Puigdoménech, M. Aragay and R. Tauler, "Comparison between
598 Different Data Pre-Treatment Methods in the Analysis of Forage Samples Using near-
599 Infrared Diffuse Reflectance Spectroscopy and Partial Least-Squares Multivariate
600 Calibration Method", *Analytica Chimica Acta* **484**, [2003].
- 601 40. J. Blasco, N. Aleixos and E. Moltó, "Machine Vision System for Automatic Quality
602 Grading of Fruit", *Biosystems Engineering* **85**, 4 [2003].
- 603
- 604
- 605

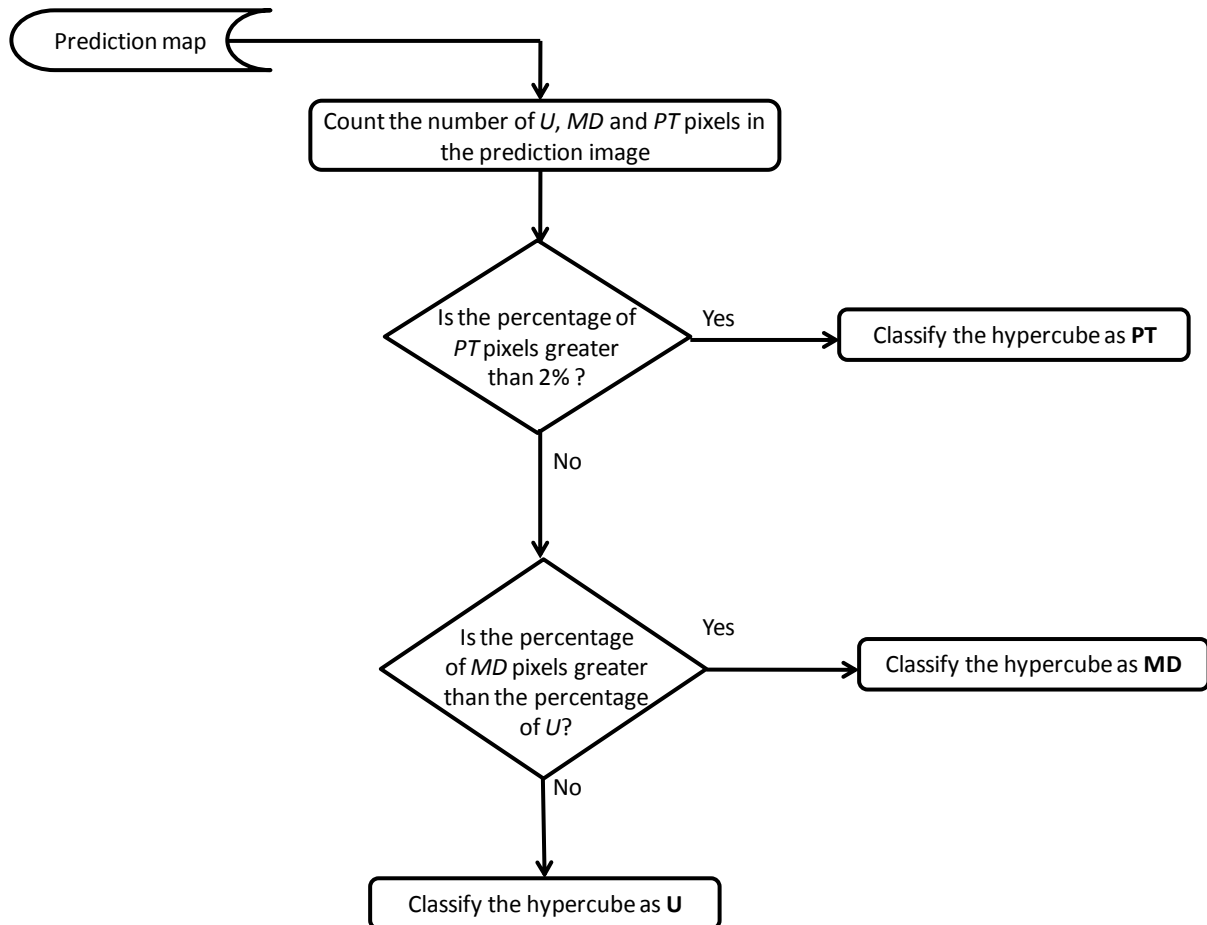
Visible Near-Infrared Hyperspectral Imaging for the Identification and Discrimination of Brown Blotch Disease on Mushroom (*Agaricus bisporus*) Caps.

E. Gaston, Jesús M. Frías, Patrick J. Cullen, Colm P. O'Donnell and Aoife A. Gowen

606 **Figures**

607 **Figure 1**

608



609

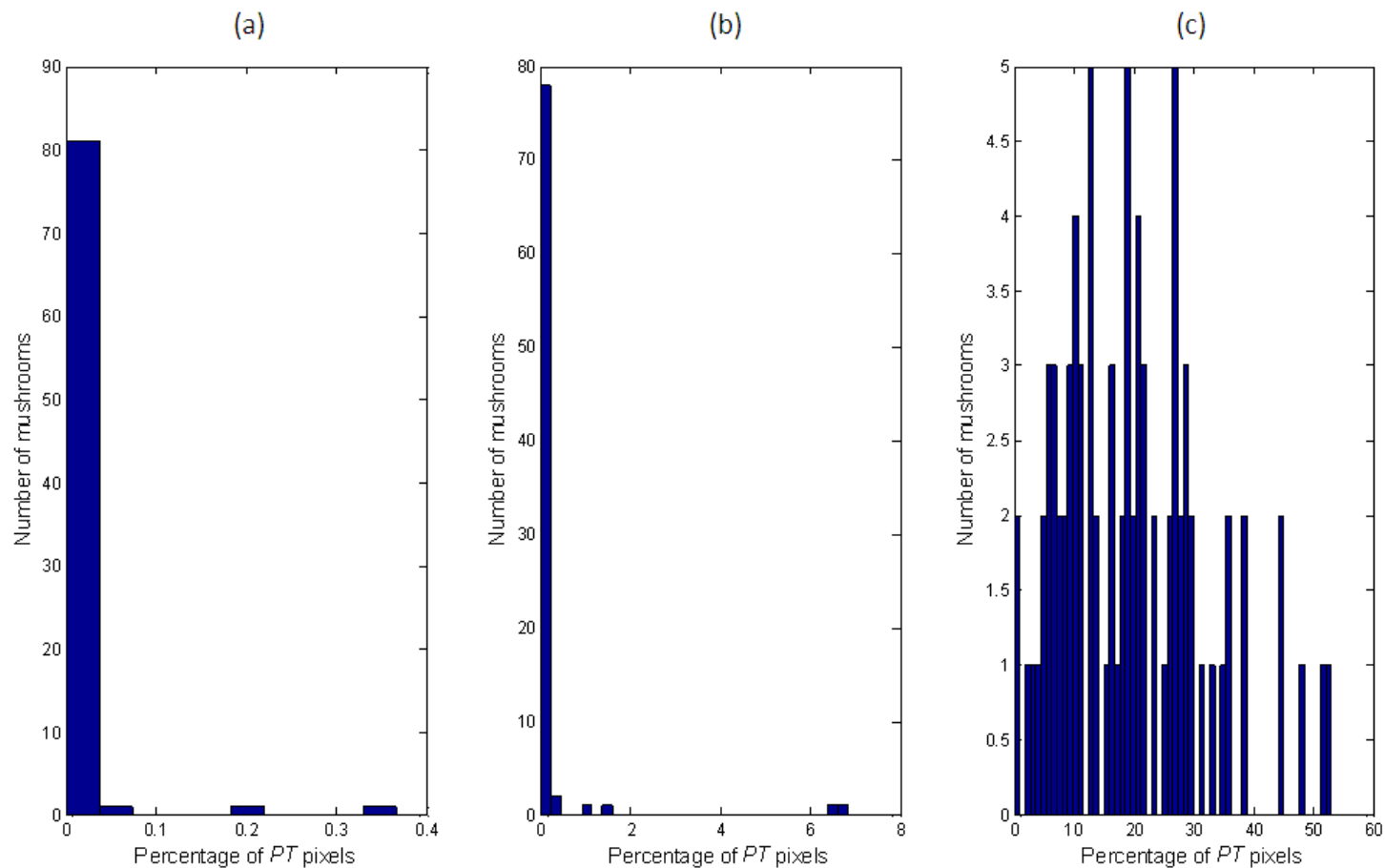
610

611 **Figure 1** Decision tree for mushroom hypercube classification, where U = undamaged, MD =
612 mechanically damaged and PT = *P. tolaasii* inoculated.

613

614

E. Gaston, Jesús M. Frías, Patrick J. Cullen, Colm P. O'Donnell and Aoife A. Gowen



615

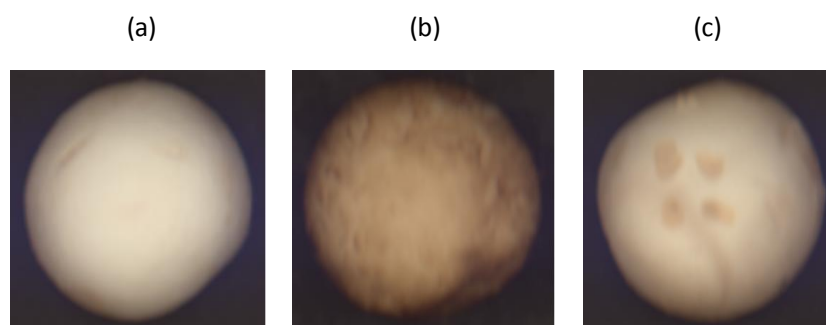
616 **Figure 2** Histograms showing number of mushrooms as a function of the percentage of pixels in the BIN_{PT} binary images of (a) undamaged (U),
617 (b) mechanically damaged (MD) and (c) *P.tolaasii* inoculated (PT) mushrooms. All the mushrooms (i.e. training and test set mushrooms) of each
618 class were plotted together, making a total of 86 samples per mushroom class.

Visible Near-Infrared Hyperspectral Imaging for the Identification and Discrimination of Brown Blotch Disease on Mushroom (*Agaricus bisporus*) Caps.

E. Gaston, Jesús M. Frías, Patrick J. Cullen, Colm P. O'Donnell and Aoife A. Gowen

619 **Figure 3**

620



621

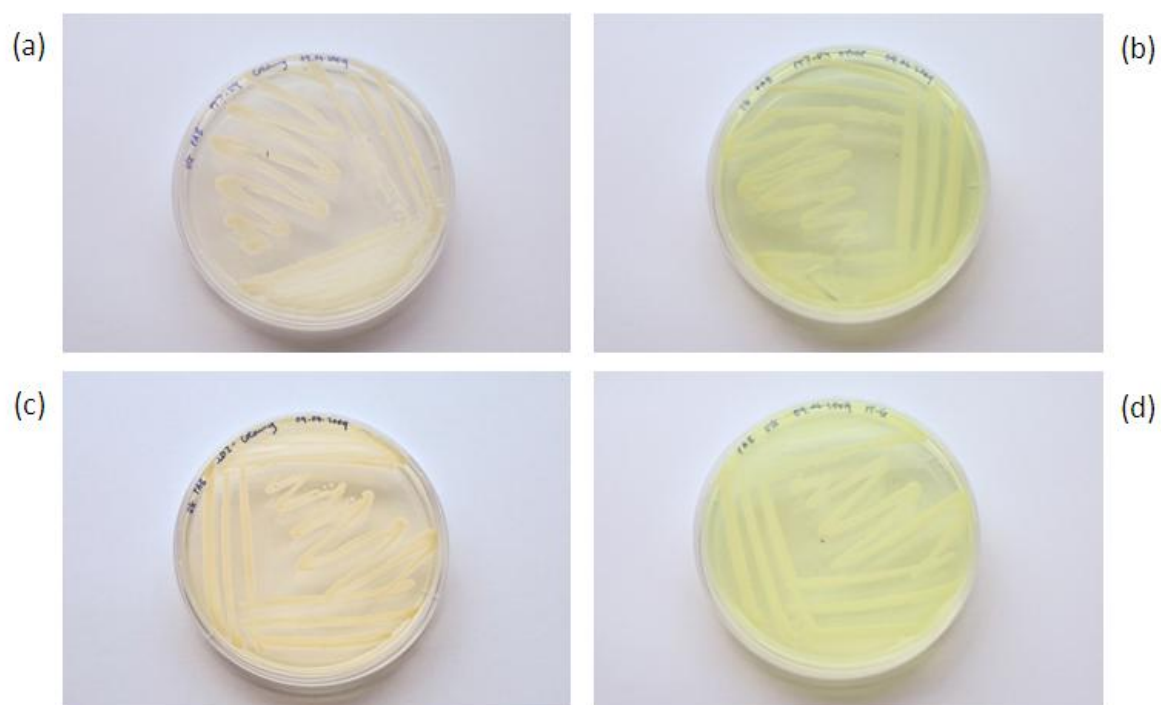
622 **Figure 3** Representative colour images of (a) undamaged (U), (b) mechanically damaged
623 (MD) and (c) *P. tolaasii* inoculated (PT) mushrooms.

Visible Near-Infrared Hyperspectral Imaging for the Identification and Discrimination of Brown Blotch Disease on Mushroom (*Agaricus bisporus*) Caps.

E. Gaston, Jesús M. Frías, Patrick J. Cullen, Colm P. O'Donnell and Aoife A. Gowen

624 **Figure 4**

625



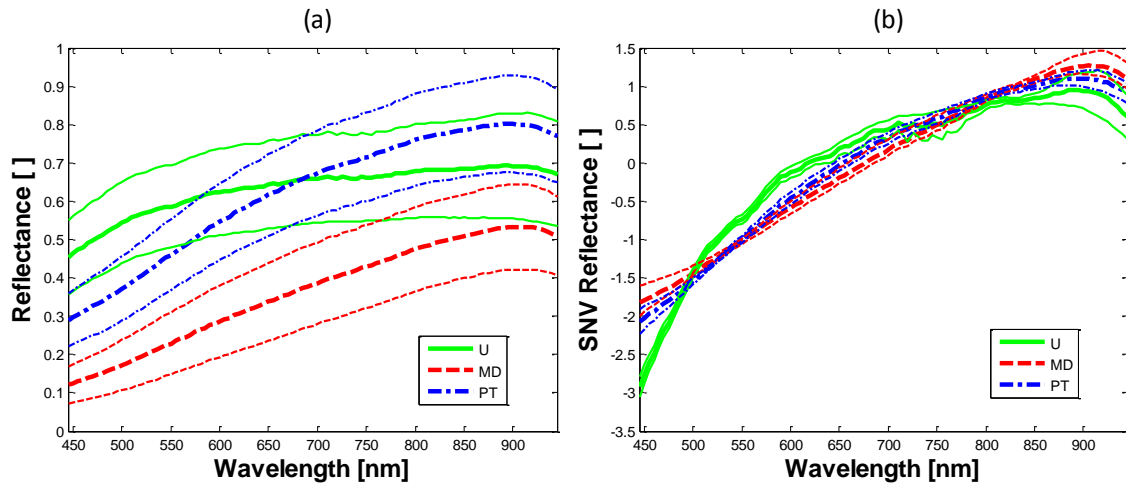
626

627 **Figure 4** (a) Creamy colonies in PAB plate of PT mushrooms, (b) Green colonies in PAB
628 plate of PT mushrooms, (c) Creamy colonies in PAB plate of U mushrooms and (d) Green
629 colonies in PAB plate of *P.tolaasii* inoculum.

Visible Near-Infrared Hyperspectral Imaging for the Identification and Discrimination of Brown Blotch Disease on Mushroom (*Agaricus bisporus*) Caps.

E. Gaston, Jesús M. Frías, Patrick J. Cullen, Colm P. O'Donnell and Aoife A. Gowen

630 **Figure 5**



631

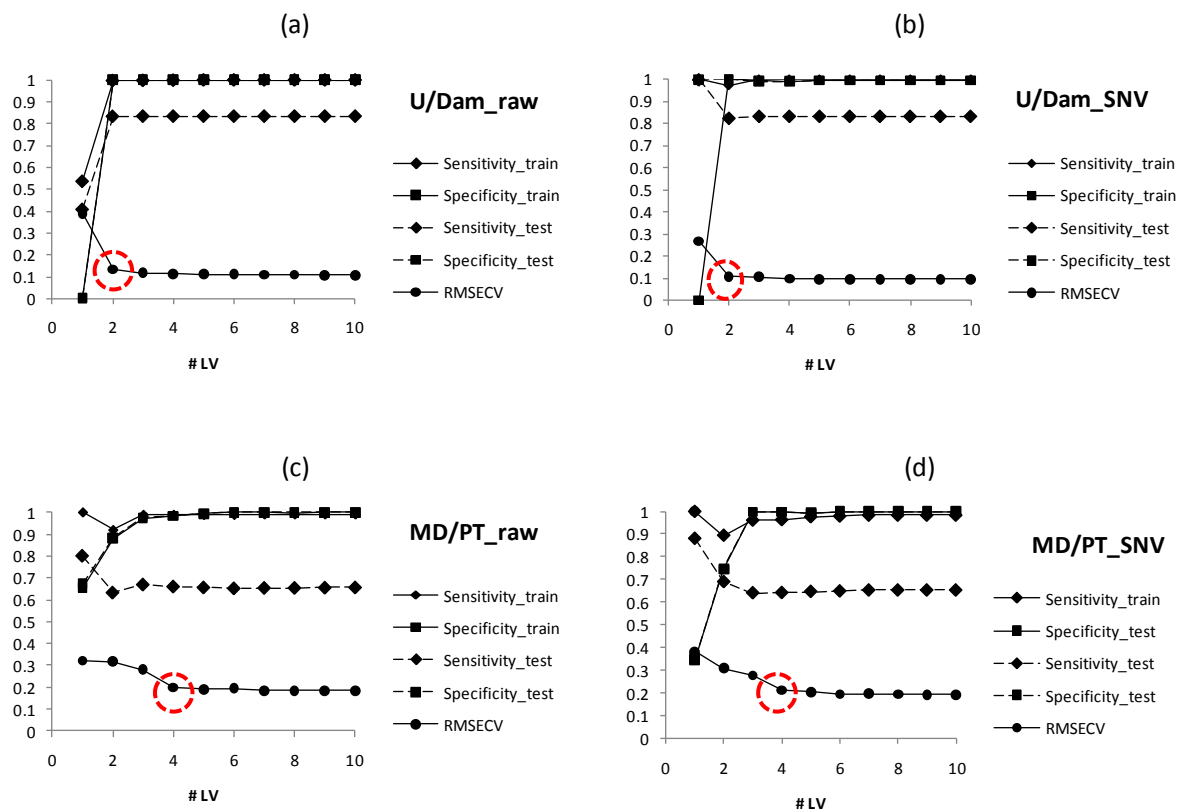
632 **Figure 5** (a) Mean \pm standard deviation raw reflectance spectra and (b) mean \pm standard
633 deviation SNV-corrected reflectance spectra of selected regions of undamaged (U),
634 mechanically damaged (MD) and *P. tolaasii* inoculated (PT) mushroom caps. For each
635 mushroom group, the broader line represents mean spectrum and the narrower lines represent
636 \pm standard deviation spectra.

637

Visible Near-Infrared Hyperspectral Imaging for the Identification and Discrimination of Brown Blotch Disease on Mushroom (*Agaricus bisporus*) Caps.

E. Gaston, Jesús M. Frías, Patrick J. Cullen, Colm P. O'Donnell and Aoife A. Gowen

638 **Figure 6**



639

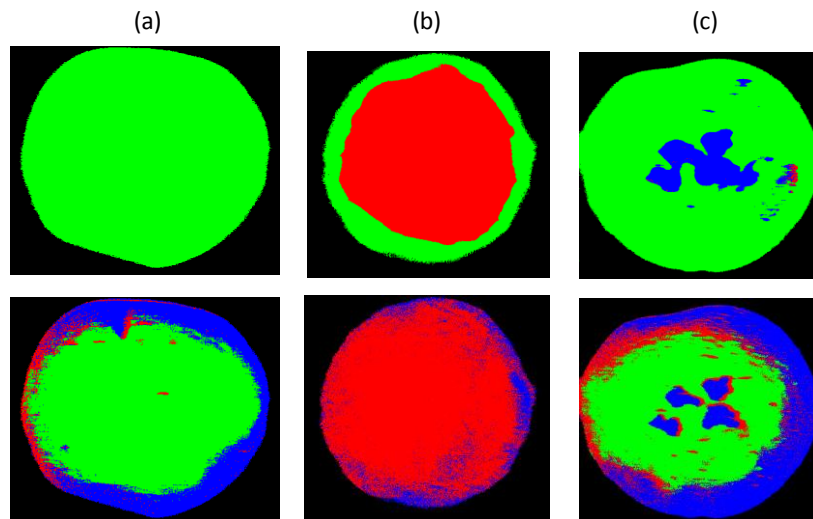
640 **Figure 6** Root-mean square error of cross-validation (RMSECV) and performance statistics
 641 (i.e. sensitivity and specificity) of PLS-DA models of (a) U/Dam_raw model, (b)
 642 U/Dam_SNV model, (c) MD/PT_raw model and (d) MD/PT_SNV model as a function of the
 643 number of latent variables (# LV), where _train = training set and _test = test set.

Visible Near-Infrared Hyperspectral Imaging for the Identification and Discrimination of Brown Blotch Disease on Mushroom (*Agaricus bisporus*) Caps.

E. Gaston, Jesús M. Frías, Patrick J. Cullen, Colm P. O'Donnell and Aoife A. Gowen

644 **Figure 7**

645



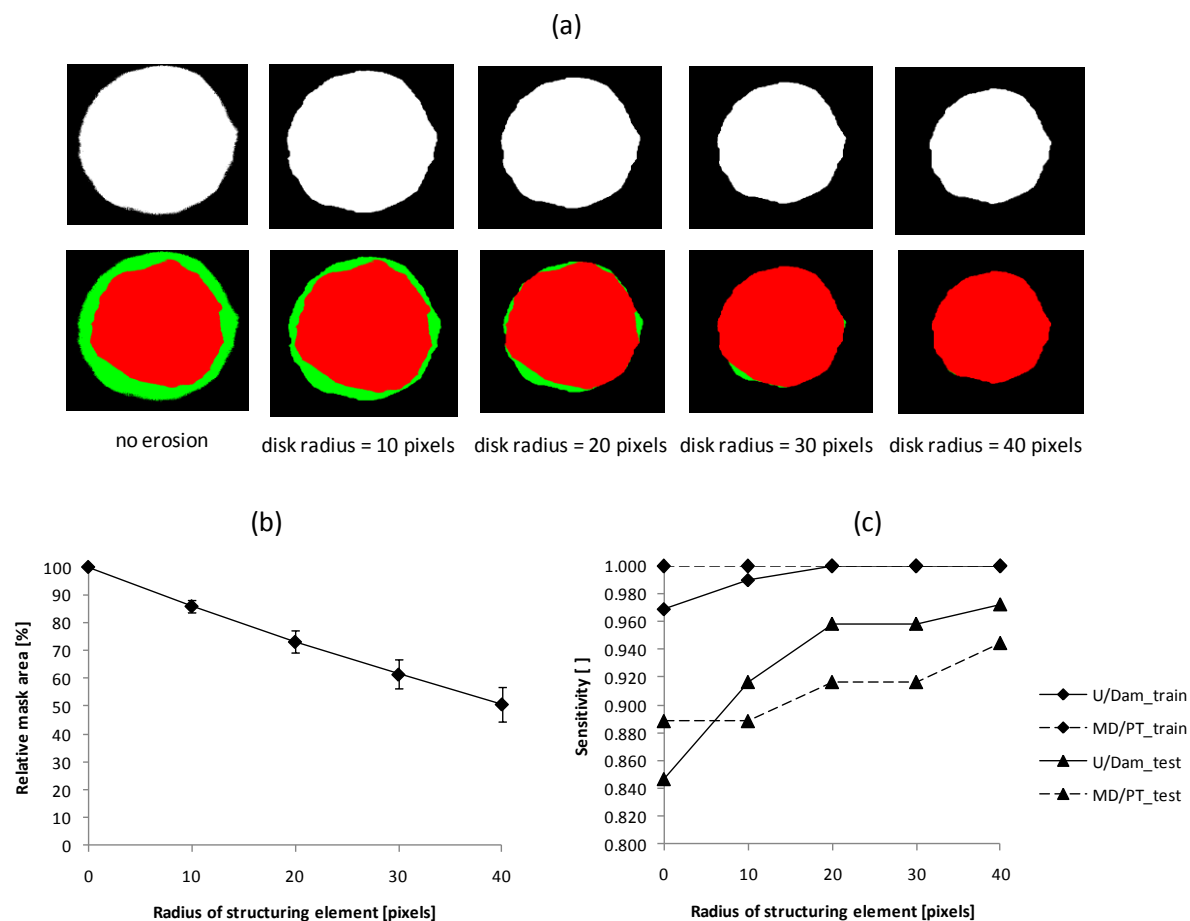
646

647 **Figure 7** Prediction images (after no erosion in Step 2) of (a) undamaged (U), (b)
648 mechanically damaged (MD) and (c) *P. tolaasii* inoculated (PT) mushrooms by PLS-DA
649 models built on raw reflectance spectra (top row) and SNV-corrected reflectance spectra
650 (bottom row).

Visible Near-Infrared Hyperspectral Imaging for the Identification and Discrimination of Brown Blotch Disease on Mushroom (*Agaricus bisporus*) Caps.

E. Gaston, Jesús M. Frías, Patrick J. Cullen, Colm P. O'Donnell and Aoife A. Gowen

651 **Figure 8**



652

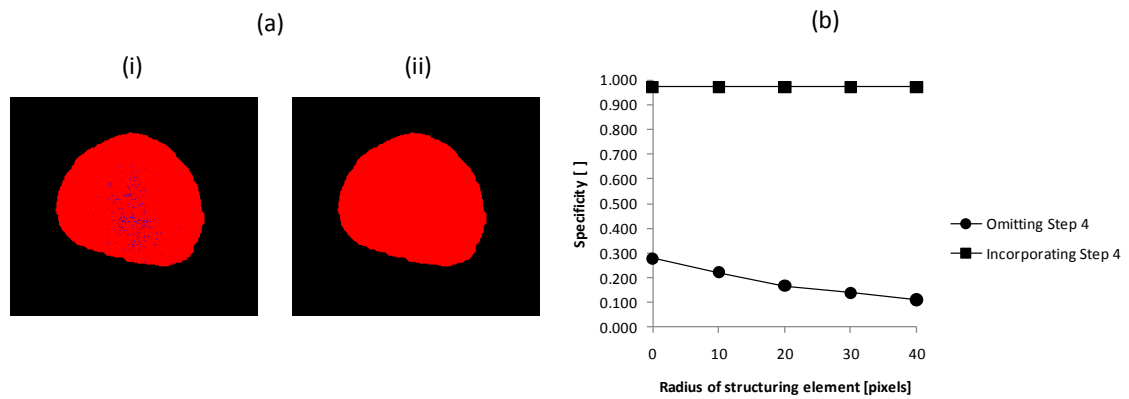
653 **Figure 8** (a) Binary masks (top row) and prediction maps (bottom row) of a mechanically
 654 damaged (MD) mushroom, (b) Average relative mask area \pm SD and (c) Sensitivity of PLS-
 655 DA models, as a function of the radius of the structuring element (SE) used for erosion in
 656 Step 2.

Visible Near-Infrared Hyperspectral Imaging for the Identification and Discrimination of Brown Blotch Disease on Mushroom (*Agaricus bisporus*) Caps.

E. Gaston, Jesús M. Frías, Patrick J. Cullen, Colm P. O'Donnell and Aoife A. Gowen

657 **Figure 9**

658



659

660 **Figure 9** Effect of the exclusion/incorporation of Step 4 to the prediction map routine in
661 terms of (a) the pixel distribution in the prediction map of a mechanically damaged (MD)
662 mushroom when (i) Step 4 was omitted and (ii) Step 4 was incorporated and (b) the
663 Specificity of the MD/PT_raw model on the test set as a function of the radius of the
664 structuring element (SE) used for erosion in Step 2.

665 .

Visible Near-Infrared Hyperspectral Imaging for the Identification and Discrimination of Brown Blotch Disease on Mushroom (*Agaricus bisporus*) Caps.

E. Gaston, Jesús M. Frías, Patrick J. Cullen, Colm P. O'Donnell and Aoife A. Gowen

666 **Tables**

667 **Table 1**

668 **Table 1** Performance statistics at spectra level of all the PLS-DA models built on reflectance
669 spectra.

Model	# LV	TRAINING SET		TEST SET	
		Sensitivity	Specificity	Sensitivity	Specificity
U/Dam_raw	2	0.997	1	0.832	1
U/Dam_SNV	2	0.973	0.999	0.825	0.999
MD/PT_raw	4	0.988	0.983	0.661	0.984
MD/PT_SNV	4	0.963	0.998	0.641	0.998

670

Visible Near-Infrared Hyperspectral Imaging for the Identification and Discrimination of Brown Blotch Disease on Mushroom (*Agaricus bisporus*) Caps.

E. Gaston, Jesús M. Frías, Patrick J. Cullen, Colm P. O'Donnell and Aoife A. Gowen

671 **Table 2**

672 **Table 2** Performance statistics at a pixel level PLS-DA models built on raw reflectance
673 spectra.

Model	TRAINING SET		TEST SET	
	Sensitivity	Specificity	Sensitivity	Specificity
U/Dam_raw	1	1	0.972	1
MD/PT_raw	1	0.979	0.944	0.972

674